Published in final edited form as:
Ann Biomed Eng. 2011 November ; 39(11): 2767–2779. doi:10.1007/s10439-011-0371-9.

A Linear, Biphasic Model Incorporating a Brinkman Term to Describe the Mechanics of Cell-Seeded Collagen Hydrogels

Peter A. Galie[1], **Robert L. Spilker**[2], and **Jan P. Stegemann**[1]

[1]Department of Biomedical Engineering, University of Michigan, 1101 Beal Ave., Ann Arbor, MI 48109, USA

[2]Department of Biomedical Engineering, Rensselaer Polytechnic Institute, Troy, NY, USA

Abstract

Protein-based hydrogels are commonly used as *in vitro* models of native tissues because they can mimic specific aspects of the three-dimensional extracellular matrix present *in vivo*. Bulk mechanical stimulation is often applied to these gels to determine the response of embedded cells to biomechanical factors such as stress and strain. This study develops and applies a linear, biphasic formulation of hydrogel mechanics that includes a Brinkman term to account for viscous effects. The model is used to predict fluid pressure, relative velocity, and estimated shear stress exerted on cells seeded within a cyclically strained collagen hydrogel with and without imposed cross flow. The model was validated using a confined compression creep test of a cardiac fibroblast-seeded collagen type I hydrogel, and the effect of the added Brinkman term was assessed. The model indicated that the effects of strain and interstitial fluid flow are strongly interdependent in the collagen hydrogel. Our results suggest that the contribution of the Brinkman term is greater in protein hydrogels than in native tissues, and that studies that apply cyclic strain to cell-seeded hydrogels should account for the induced interstitial fluid flow. This study, therefore, has relevance to the increasing number of studies that examine cellular responses to mechanical stresses using *in vitro* hydrogel models.

Keywords

Collagen gel; Mechanics; Hydrogel; Finite element modeling; Brinkman term

Introduction

Cell-seeded collagen hydrogels have been used for decades as *in vitro* models of biological tissues.[1,3,8,14] Hydrogels provide a controlled, three-dimensional environment that can be used to imitate several components of the milieu surrounding cells in the body. These gels, or those consisting of similar natural polymers, are often exposed to tensile, compressive, and shear stresses in order to understand the effect of mechanical stress on the phenotype of cells in 3D.[10,11,13,28,29] Determining the local stress or strain environment at the cellular level is often complicated by the viscoelastic and nonlinear mechanics of the gels. In addition, protein- and polysaccharide-based hydrogels have very high porosities (often >95%) in the hydrated state. Therefore, the stress exerted on cells has both a fluid and a

Address correspondence to Jan P. Stegemann, Department of Biomedical Engineering, University of Michigan, 1101 Beal Ave., Ann Arbor, MI 48109, USA. jpsteg@umich.edu.

Associate Editor Konstantinos Konstantopoulos oversaw the review of this article.

solid component. Because of the dual nature of the stress state, a biphasic formulation of the fluid and structural constitutive equations can provide the basis for a finite element model describing the stresses within the hydrogel.

Originally applied to cartilaginous tissue, biphasic theory has been used in the biomedical field for nearly 30 years, as pioneered[23] and extended by Mow *et al.*[21] This biphasic model is derived from mixture theory[4,17,19] and couples intrinsically incompressible solid and fluid phases. In its simplest form it yields a time-dependent, viscoelastic-like response related to the flow of the fluid phase relative to the solid phase. In virtually all applications of this model to physiological tissues such as cartilage, a Darcy equation that does not account for viscous effects is used. Consequently, such models are unable to describe shear stresses exerted by the interstitial fluid. Subsequent models have been derived that add increased sophistication to the original linear model, including nonlinear deformation, intrinsic viscoelasticity of the solid phase, anisotropy, as well as the addition of a Brinkman term to the fluid constitutive equation.[6,18,27] The Brinkman term comes from the Brinkman equation, which is a semi-empirical equation that accounts for viscous effects of interstitial fluid. Using the biphasic formulation in the absence of the Brinkman term, fluid velocity is derived from the solved values of fluid phase pressure and solid displacement. Biphasic models incorporating a Brinkman term have been used to analyze viscous effects at the interface between fluid and biphasic domains, for example to develop theoretically consistent boundary conditions and study interactions between cartilage and synovial fluid boundaries in articulated joints.[2,18] However, these studies have largely concluded that the Brinkman term can be neglected when considering the response within physiological tissues like cartilage.

This study incorporates a Brinkman term into biphasic theory to create a finite element model that estimates stresses within mechanically stimulated protein hydrogels. Previous studies have used computational models to estimate stresses within fibrillar collagen matrices,[31] as well as stress exerted on cells embedded within various soft tissues.[5,30] For example, a recent study used neo-Hookean strain energy density functions to describe the structural deformation of dermal tissue, and used the calculated strain of cell membranes to determine calcium uptake through stretch-mediated channels.[26] Biphasic models have also been used to determine stress exerted on chondrocytes.[16] These models have illuminated the complexity of cell–matrix interactions at the microscale.

The model described here assumes a biphasic continuum and does not simulate the cells and extracellular matrix individually. The solid phase was modeled using linear deformation theory, and the fluid component model included a Brinkman term to account for viscous effects. A main goal of this study was to determine whether inclusion of a Brinkman term increased the utility of the biphasic model in predicting the mechanical behavior of hydrogels. The 2D model was validated by predicting the creep behavior of a cell-seeded gel in confined compression. The computational results were compared to experimental results to examine the significance of this term in predicting the behavior of collagen hydrogels. The model was then further applied to estimate stresses within a cyclically stretched cell-seeded hydrogel, and specifically to determine how the stress state within the gel changed between three testing configurations: strain only, cross flow only, and combined strain and flow. The results of this study illuminate differences in the mechanical behavior of protein hydrogel tissue analogs and native tissue mechanics, and also have utility in estimating stress and strain levels in engineered tissues.

Experimental Methods

Gel Preparation and Flow-Strain Apparatus

Collagen type I hydrogels were prepared using a method described in a previous study.[12] Briefly, acid-solubilized bovine collagen type I (MP Biomedicals, Solon, OH) was diluted to a final concentration of 2.0 mg/mL with 10% FBS, DMEM, and 0.1 M NaOH at physiological pH on ice. Rat cardiac fibroblasts were suspended in the cold liquid collagen solution at a concentration of 0.5×10^6 cells/mL. These cells, which range in size between 30 and 60 μm, were chosen because they have been used for previous measurements of gel properties.[12] For both gel parameter testing and the creep validation, gel solution was polymerized in 24- or 12-well plates, respectively. For use in the previously described flow/strain apparatus,[11] 0.7 mL of the suspension was placed on top of previously polymerized 0.3 mL of acellular 2.0 mg/mL collagen. Gelation was then initiated at 37 °C in a humidified 5% CO_2 to create a homogeneous, cell-seeded 3D collagen hydrogel. The construction and preparation of the flow-strain apparatus, including the acid etching used to facilitate gel attachment and flow visualization to validate the layering approach, has been described in a previous study.[11] Briefly, axial strain is applied to the PDMS wells during simultaneous cross flow imposed by a syringe pump delivering 10 μL/min of culture medium. A strain magnitude of 5% was chosen because previous studies have shown that strains as small as 3% can stimulate a significant effect on cardiac fibroblasts.[15] The PDMS wells are within a culture medium bath that is kept at 37 °C and physiological pH using 2-[4-(2-hydroxyethyl)piperazin-1-yl]ethane-sulfonic acid (HEPES) buffer.

Model Parameters

The parameters incorporated into the computational model include the elastic modulus, Poisson's ratio, permeability, and porosity of the hydrogel, in addition to the viscosity of the fluid within the gel. Gel properties were measured after 24 h of incubation at 37 °C and 5% CO_2. The elastic modulus was measured in unconfined compression, using a 30%/s strain rate to 30% strain. The elastic modulus was calculated by taking the slope of the resulting stress–strain curve near 10% strain to assure the validity of the infinitesimal strain assumption. After an initial toe-in region, the stress–strain curve was linear in this strain regime. To determine the Poisson's ratio, the same unconfined compression setup was used to control strain in the *y* direction and the resulting radial strain was measured optically using ImageJ software.

The permeability of cell-seeded gels was also measured in a previous study, and was found not to significantly depend on strain for values ≤5%.[11] Strains larger than 5% may certainly affect permeability, as detailed by previous studies.[7,22,24] Porosity can be determined from the collagen concentration in the hydrogels, using a formula presented in a previous study[25] that takes into account the specific gravity of the collagen. Since the collagen concentration was 2.0 mg/mL, or 0.2% weight/volume, the porosity was calculated to be 99.6%. The fluid in the gel is primarily water, so the viscosity was assumed to be equal to that of water, 0.1 cP at 25 °C.

Confined Compression

2.0 mL hydrogels were created in standard 12-well plates, and after 24 h transferred to a compression chamber confined to restrict strain in the radial direction during axial compression. The inner diameter of the chamber was machined to have the same diameter as the plate wells, so the sides of the gel contacted the walls of the compression chamber. The top platen consisted of a stainless steel plate with through holes of 1 mm diameter spaced apart by 2 mm (center to center), to allow fluid to escape the gel during compression. An image and schematic of this setup are shown in Figs. 1a and 1b, respectively. The resistance

to fluid flow through the platen was considered negligible. The boundary conditions used for the validation simulation are shown in Fig. 1c. A uniaxial testing system was used to apply a constant load of approximately 280 N for 10 min. The creep rate was determined by taking the slope of the strain-time curve near the 5 min time point, when the curve was linear and the strain was held < 10% to maintain the linear deformation assumption.

Viscous Biphasic Formulation

For purposes of the following presentation, assume standard tensor notations, Cartesian coordinates, x_i, i = 1, 2, 3, a comma to denote spatial differentiation (e.g., $u_{ij} = \partial u_i/\partial x_j$), and a dot for a time derivative (e.g., $\dot{u}_i = \partial u_i/\partial t$). Superscripts s and f refer to the solid and fluid phases, respectively. Biphasic theory[17] assumes that the medium is saturated, so that the solid and fluid fractions (solidity and porosity, respectively) sum to unity, and for linear models are constants:

$$\varphi^{\mathrm{s}}+\varphi^{\mathrm{f}}=1 \tag{1}$$

where φ is the volume fraction. The conservation of mass was expressed as a function of both the porosity and solidity. Continuity was described by:

$$(\varphi^{\mathrm{s}}\dot{u}_l^{\mathrm{s}}+\varphi^{\mathrm{f}}\dot{u}_i^{\mathrm{f}}),i=0 \tag{2}$$

where u is displacement. The solid and fluid constitutive equations were given by:

$$\sigma_{ij}^{\mathrm{s}}=-\varphi^{\mathrm{s}}p\delta_{ij}+\frac{1}{2}C_{ijkl}\left(u_{i,j}^{\mathrm{s}}+u_{j,i}^{\mathrm{s}}\right) \tag{3}$$

$$\sigma_{ij}^{\mathrm{f}}=\varphi^{\mathrm{f}}p\delta_{ij}+\frac{\mu}{2}\left(\dot{u}_{i,j}^{\mathrm{f}}+\dot{u}_{j,i}^{\mathrm{f}}\right) \tag{4}$$

where p is the fluid phase pressure and σ_{ij} represents the Cauchy stress tensor, since the present model assumes linear deformations. C_{ijkl} represents the stiffness tensor of the solid phase, which consists of only the elastic modulus and Poisson's ratio of the hydrogel, since the model also assumes isotropy. The fluid constitutive equation incorporated a Brinkman term to account for the effects of fluid viscosity, μ. The momentum balances for the solid and fluid fractions were expressed as follows:

$$\sigma_{ij,j}^{\mathrm{s}}+\frac{\varphi^{\mathrm{f}^2}}{k}(\dot{u}_i^{\mathrm{f}}-\dot{u}_i^{\mathrm{s}})=0 \tag{5a}$$

$$\sigma_{ij,j}^{\mathrm{f}}-\frac{\varphi^{\mathrm{f}^2}}{k}(\dot{u}_i^{\mathrm{f}}-\dot{u}_i^{\mathrm{s}})=0 \tag{5b}$$

where k represents the permeability of the medium, in units of (m^3s/kg). Boundary conditions complete the mathematical description and will be taken up separately below.

Kinetic Boundary Conditions

To describe the boundaries between the biphasic domain and impermeable walls, conditions for both the solid displacement and fluid velocity must be specified. Roller constraints, which restrict solid displacement normal to the wall but allow frictionless parallel deformation were applied to these interfaces:

$$u_i^s n_i = 0 \quad \text{on} \Gamma_{\text{roller}} \tag{6}$$

where n is the unit normal vector and Γ represents the boundary. A traditional no-slip condition was not appropriate for specifying the fluid velocity at the wall in our viscous biphasic formulation. However, the fluid must have zero velocity relative to the solid fraction, even if the solid fraction is deforming. Previous models have applied a “pseudo-no-slip” condition to describe this viscous biphasic kinetic boundary condition.[6,18] These references provide a full explanation of the theory supporting this condition, and it is typically implemented by setting the weighted velocity equal to zero at all stationary biphasic–solid interfaces:

$$\dot{u}_i^w = \varphi^s \dot{u}_i^s + \varphi^f \dot{u}_i^f = 0 \quad \text{on} \Gamma_{\text{noslip}} \tag{7}$$

However, when the wall itself has a velocity, this condition is invalid. In this case, to prescribe no flow at the boundary ($\dot{u}_i^f - \dot{u}_i^s = 0$) the weighted velocity was set to the solid velocity of the wall:

$$\dot{u}_i^w = \dot{u}_i^s \quad \text{on} \Gamma_{\text{noslip-moving wall}} \tag{8}$$

Kinematic Boundary Conditions

To describe open boundaries on the biphasic domain (i.e., a free draining condition for confined compression), fluid phase tractions must be set at the boundary. The following condition from a previously published model[18] was used:

$$\sigma_{ij}^f n_j = \varphi^f \sigma_{ij}^\Omega n_j \tag{9}$$

where σ_{ij}^Ω is the prescribed fluid phase stress at the boundary. Since an open boundary by definition has zero-fluid phase stress at the boundary, Eq. (9) reduced to the following:

$$\frac{\sigma_{ij}^f}{\varphi^f} = 0 \quad \text{on} \Gamma_{\text{open}} \tag{10a}$$

In order to prescribe interstitial cross-flow condition at a boundary, the same formula can be used and the fluid phase stress set to the applied pressure:

$$\frac{\sigma_{ij}^{\mathrm{f}}}{\varphi^{\mathrm{f}}}=P \ \ \mathrm{on}\Gamma_{\mathrm{delP}} \tag{10b}$$

Inviscid Formulation

To reduce the viscous biphasic formulation to an inviscid biphasic model, the Brinkman term was removed from the governing equations. Removing the viscous term reduced Eq. (5b) to the following:

$$\sigma_{ij}^{\mathrm{f}}=-\varphi^{\mathrm{f}}p\delta_{ij} \tag{11}$$

By removing this term, fluid velocity became a derived variable, and the dependent variables reduced to the solid displacement and fluid pressure, as in standard linear biphasic analyses. However, when using roller boundaries, the boundary conditions changed slightly. Since fluid/weighted velocity is no longer a primary variable, a nonslip condition was unnecessary. Rather, a zero-flux condition was applied at these surfaces. Moreover, setting a free draining boundary at the top surface was accomplished by simply setting fluid pressure to zero at this boundary. Also, pressure for a cross-flow condition was set directly. These boundaries conditions are expressed below:

$$Q=\varphi^{\mathrm{f}}(\dot{u}_l^{\mathrm{f}}-\dot{u}_l^{\mathrm{s}})=0 \ \ \mathrm{on}\Gamma_{\mathrm{zeroflux}} \tag{12}$$

$$p=0 \ \ \mathrm{on}\Gamma_{\mathrm{open}} \tag{13a}$$

$$p=P \ \ \mathrm{on}\Gamma_{\mathrm{delP}} \tag{13b}$$

It can be shown that these boundaries are identical to the viscous formulation for zero viscosity.

Computational Implementation of Governing Equations

COMSOL Multiphysics software version 3.5a was used to construct the finite element formulation for the biphasic model with viscosity. COMSOL implementation involves defining an appropriate set of unknown primary variables, defining the governing equations in terms of those variables, and then modifying built in equations in COMSOL to provide the exact viscous biphasic equations internally, with appropriate coupling. Three governing equations were required to describe the biphasic medium in COMSOL: the continuity equation (Eq. 2) and conservation of momentum equations for both the solid and fluid phases. In order to implement this in the COMSOL software, the conservation equations were described in terms of the three selected variables, solid displacement, fluid pressure, and weighted velocity. The continuity equation is already in terms of weighted velocity, and

needed no further manipulation. However, to find the conservation of solid momentum, Eq. (3) was substituted into Eq. (5a) to produce:

$$-\varphi^{s} p,i+C_{ijkl}\left(u^{s}_{(i,j)}\right)_{,j}+\frac{\varphi^{f}}{k}(\dot{u}^{w}_{i}+\dot{u}^{s}_{l})=0 \tag{14}$$

Similarly, the conservation of fluid momentum was derived by substituting Eq. (4) into Eq. (5b).

$$-\varphi^{f} p,i+\frac{\mu}{\varphi^{f}}\left(\dot{u}^{w}_{(i,j),j}+(\varphi^{f}-1)\dot{u}^{s}_{(i,j),j}\right)-\frac{\varphi^{f}}{k}(\dot{u}^{w}_{i}-\dot{u}^{s}_{l})=0 \tag{15}$$

As expected, for a rigid medium in which there is no solid displacement, Eq. (15) simplified to the Brinkman equation.

Equations (2), (14), and (15) sufficiently describe the viscous biphasic medium, and all three equations are functions of weighted velocity, solid displacement, fluid pressure, or a combination of these variables. Quadratic shape functions were utilized to discretize the equations, and the direct, linear solver “unsymmetric multifrontal sparse LU factorization package” (UMFPACK) was used to find a time-dependent solution. UMFPACK was chosen because of its ability to solve unsymmetric linear systems.

Boundary Condition Implementation

The boundary conditions must also be implemented in the COMSOL software. The roller constraints were applied directly, since solid displacement was a selected variable. The same can be said for the pseudo-no-slip condition and the weighted velocity. However, to apply the open or cross-flow boundary conditions in COMSOL, several manipulations were necessary. For a general stress boundary, COMSOL allowed for the input of f_0, the applied force at the boundary:

$$\frac{1}{\varphi^{f}}\sigma^{f}_{ij}n_{j}=f_{0}n_{i}-\frac{\mu\varphi^{s}}{\varphi^{f}}\dot{u}^{s}_{(i,j)}n_{j} \tag{17}$$

Substituting Eq. (10a), the open boundary condition was implemented by setting the normal force, F_i:

$$F_{i}=f_{0}n_{i}=\frac{\mu\varphi^{s}}{\varphi^{f}}\dot{u}^{s}_{(i,j)}n_{j} \tag{18a}$$

Likewise, cross flow was implemented by adding the set pressure directly to Eq. (17):

$$F_{i}=f_{0}n_{i}=\frac{\mu\varphi^{s}}{\varphi^{f}}\dot{u}^{s}_{(i,j)}n_{j}+P \tag{18b}$$

Prescribing solid phase tractions on a boundary in COMSOL required that the software's definition of solid traction, t_i^{COSMOL}, be modified, as it contains only the stress from solid phase displacement:

$$t_i^{\mathrm{COSMOL}} = \frac{1}{2} C_{ijkl} \left(u^{\mathrm{s}}_{i,j} + u^{\mathrm{s}}_{j,i} \right) n_j \tag{19}$$

In order to be consistent with our biphasic definition, we defined total traction as:

$$\begin{aligned} t_i^{\mathrm{Total}} &= \sigma_{ij}^{\mathrm{Total}} n_j = \left(\sigma^{\mathrm{s}}_{ij} + \sigma^{\mathrm{f}}_{ij} \right) n_j \\ &= -p\delta_{ij} n_j + \tfrac{1}{2} C_{ijkl} \left(u^{\mathrm{s}}_{i,j} + u^{\mathrm{s}}_{j,i} \right) n_j + \tfrac{\mu}{2} \left(\dot{u}^{\mathrm{f}}_{i,j} + \dot{u}^{\mathrm{f}}_{j,i} \right) n_j \end{aligned} \tag{20}$$

Combining Eqs. (19) and (20), we prescribed traction consistent with the COMSOL implementation of the biphasic domain via:

$$t_i^{\mathrm{COSMOL}} = t_i^{\mathrm{Total}} + p\delta_{ij} n_j - \frac{\mu}{2} \left(\dot{u}^{\mathrm{f}}_{i,j} + \dot{u}^{\mathrm{f}}_{j,i} \right) n_j \tag{21}$$

Equation (21) required that traction be defined in COMSOL in terms of the prescribed total traction (first term, known) as well as the pressure and fluid-phase strain rate, both of which were unknown. The software calculated these two fields so that they properly satisfied the traction condition. Prescribing a solid traction for the inviscid model was executed in a similar manner, with the exception that the fluid stress tensor did not include a viscous term. Hence, for an inviscid formulation, Eq. (21) reduced to the following:

$$t_i^{\mathrm{COSMOL}} = t_i^{\mathrm{Total}} + p\delta_{ij} n_j \tag{22}$$

Matching Boundary Conditions to Experimental Apparatus

A schematic of the location of the cell-seeded gel within the PDMS wells of the flow-strain system is shown in Fig. 2a, and is described further in our previous work.[11] The cell-seeded gel was polymerized on top of an acellular gel, which was used to distribute fluid flow entering the PDMS well. The cell-seeded hydrogel was bounded on the left and right by the sides of the PDMS, and below by the acellular gel, which was about 4-fold thicker than the cellular gel. For cases involving an imposed cross flow of 10 μL/min, the pressure drop across the gel was calculated using Darcy's equation and the thickness and permeability of the gel, and was shown to be approximately 77.6 Pa. A summary of the boundary conditions for the strain, flow, and combined strain and flow configurations is shown in Figs. 2b–2d. For all cases, the right boundary was held fixed (to simulate gel attachment to the PDMS), the top boundary is open to atmosphere, and the bottom boundary was supported by rollers (to simulate attachment to the acellular gel while allowing deformation in the direction of strain). At unconstrained boundaries, the solid phase stress was set to zero and at all boundaries, the solid phase shear stress was set to zeroAt unconstrained boundaries, the solid phase stress was set to zero $(\sigma^{\mathrm{s}}_{xx} = \sigma^{\mathrm{s}}_{yy} = 0)$ and at all boundaries, the solid phase shear stress was set to zero $(\sigma^{\mathrm{s}}_{xy} = 0)$.

Calculating Variance of Model Predictions

As the model incorporated measured values of parameters including elastic modulus, Poisson's ratio, and permeability, its predicted creep rate also had a variance. In order to calculate the magnitude of this variance, the simulation was run using the average values of these measured parameters as well as with values ±1 SD of the measurement. The standard deviation of the model prediction was calculated by taking the difference between the creep rate calculated using average parameter values and that produced by parameters ±1 SD.

Results

Using values for elastic modulus, Poisson's ratio, permeability, and porosity for the cell-seeded gels at the 24 h time point, the model was used to predict the creep rate of the gels in confined compression. These values were compared to experimental measurements obtained by applying several different stress magnitudes to collagen hydrogels and determining resulting creep rates, using the boundary conditions described in Fig. 1c. In the experimental studies, an average creep rate of $2.48E{-}3 \pm 5.12E{-}4$ $kPa^{-1}s^{-1}$ was measured using the confined compression test apparatus, where creep rate was defined as the deformation of the top surface of the gel per unit time and per applied stress. The 2D biphasic model incorporating the Brinkman term predicted a normalized creep rate of $2.525E{-}3 \pm 2.44E{-}4$ kPa^{-1} s^{-1}, which was 1.4% higher than the experimental value. To test the importance of adding the viscous term in the biphasic simulation, the model was run again using a linear biphasic formulation. This inviscid simulation yielded a creep rate of $3.35E{-}3 \pm 1.68E{-}4$ kPa^{-1} s^{-1}, a value 35% higher than the experimentally determined value.

Using the creep rate comparison as validation of the viscous biphasic formulation, the model was then used to predict fluid pressure within the hydrogel during cyclic strain. To further analyze the effect of the Brinkman term, fluid pressures were also calculated using the inviscid linear biphasic formulation. A comparison of the fluid pressure within the gel during half of one cycle of 5% tensile strain with and without the Brinkman term is shown in 2D contour maps shown in Figs. 3a and 3b, respectively. When incorporating the Brinkman term, the calculated pressure was considerably increased, with the peak pressure occurring at the end of the gel being deformed. The contour plots display a small region of high pressure area that dissipates as the gel expands. This contrasts with the inviscid formulation, which predicts a symmetric pressure distribution with respect to the *y*–*z* plane throughout the loading cycle. Figures 4a and 4b plot the pressure profile along the *x* axis centerline of the gel during this strain cycle with and without the Brinkman term. Away from the boundary being strained, the pressure profile between the Brinkman and linear formulations appeared quite similar. These plots again demonstrated the symmetry of the linear formulation, which did not capture the rise in pressure near the cycling end of the gel, and appeared to be approximately constant with respect to the *x* coordinate. To assess the importance of the Brinkman term over a range of permeability values, the pressures at the *y* axis centerline of the gel were averaged for formulations with and without the term, and Fig. 4c shows the average ratio between the two predictions. For a range of permeabilities between $0.25E{-}11$ and $5.0E{-}11$ m^3s/kg, the addition of the Brinkman term substantially affected the predicted pressure. For the highest permeability value ($k = 5.0E{-}11$ m^3s/kg), the formulation excluding the Brinkman term overestimated the fluid pressure along the *y* axis centerline.

To determine the effects of parameters like porosity and permeability on the predicted fluid pressure and velocity, different values were input into the model. As Fig. 5a indicates decreasing the porosity by a factor of two ($\varphi = 0.498$) while keeping the permeability constant did not substantially affect the pressure distribution along the *x* axis centerline of the gel at 5% strain. The only difference appeared near the end of the gel being cycled, while changing the permeability by a factor of two ($k/2 = 0.715E{-}11$ m^3s/kg, $2{*}k = 2.86E{-}11$

m^3s/kg) had a much larger effect on pressure. As expected, permeability inversely affected the fluid pressure and relative velocity in the *y* direction (Fig. 5b). In contrast to its effect on fluid pressure, porosity had a greater effect on the relative fluid velocity.

Based on the established importance of adding the viscous Brinkman term to the biphasic model for hydrogels, we then used the full model to determine the differences in pressure, relative fluid velocity, and von Mises stress distributions caused by adding a cross flow to the gel, both with and without applied cyclic strain. Figures 6a and 6b show the pressure distribution along the centerline parallel to the *y* direction for cyclically strained gels, without and with the addition of cross flow, respectively. Addition of cross flow superimposed a pressure gradient on the pressure distribution caused by strain alone (Fig. 6b). For both solutions, the pressure at the top boundary of the gel was fixed at zero. However, for the cross-flow solution, the pressure at the bottom boundary was constant at the applied pressure of 77.6 Pa throughout the strain cycle. As expected, the pressure distribution became progressively more negative as the gel expanded.

As a comparison, the modeled pressure and fluid velocity profiles in hydrogels exposed only to cross flow are shown in Figs. 7a and 7b. The gel experienced negligible deformation from the applied pressure gradient compared to the gels that were cyclically strained. The simulation predicted an almost linearly decreasing pressure profile through the centerline of the gel (Fig. 7a) and a relatively constant fluid velocity in the *y* direction of approximately 1 μm/s (Fig. 7b). This is the pressure drop and *y* velocity expected for a simple Darcy flow for the given pressure drop. Conversely, the fluid velocity in the gels exposed to cyclic strain, with and without cross flow, indicated that strain produced velocities ranging from about −10 to +10 μm/s (an order of magnitude higher than the static cross-flow case). Plots of these strain-induced velocities along the gel midpoint in the *x* direction are shown in Figs. 8a and 8b for three time points during the 5% tensile strain cycle without and with cross flow. The plots indicate that without the addition of cross flow, there is no relative fluid velocity in the middle of the gel; fluid enters and exits the top and bottom boundaries, but there is no net relative fluid flow across the length of the gel in the *y* direction. Conversely, the addition of cross flow induces a relatively constant relative fluid flow in the *y* direction. Because of the addition of the Brinkman term, the relative fluid velocity is zero at the left and right boundaries. The relative fluid velocities can be used to estimate shear stress caused by the fluid flow on cells within the gel. Figures 9a–9c show the results of this calculation along the midpoint of the gel in the *y* direction for strain only (Fig. 9a), strain and cross flow (Fig. 9b), and cross flow only (Fig. 9c). To determine shear stress from relative fluid flow, an equation derived by Wang and Tarbell[32] in a previous study of interstitial flow-induced shear stress on embedded cells was used:

$$\tau_i = \frac{\mu}{k}\varphi^{\mathrm{f}}(u_i^{\mathrm{f}} - u_i^{\mathrm{s}}) \tag{30}$$

For the cross flow-only condition, there was a constant shear stress of about 0.1 dyn/cm^2 in the *y* direction. For the cases involving strain, the shear stress oscillated between −1 and 1 dyn/cm^2. The only difference caused by the addition of cross flow was manifested in a 0.1 dyn/cm^2 increase in shear stress throughout the cycle.

The von Mises stress, a scalar measure of the combined principal stresses, can be computed from the solid stress tensor defined in Eq. (3) and analyzed for the three different stimulation scenarios. These stress distributions are shown in Figs. 10a–10c for a centerline along the *x* component of the gel for strain only (Fig. 10a), strain and cross flow (Fig. 10b), and cross flow only (Fig. 10c). As expected for the cases involving strain, the stress peaked near the

left boundary of the gel for each point in the strain cycle, corresponding to the pressure rise in Fig. 4a. Interestingly, the addition of cross flow to cyclic strain did not substantially affect the von Mises stress, indicating that the stress induced by the cyclic strain-dominated stress induced by the cross flow. Finally, the von Mises stress for the cross flow-only condition was about an order of magnitude less than the other conditions. This result implies that the strain caused by the cross flow was much less than the strain caused by the cyclic deformation of the gels.

Discussion

The results of this study demonstrate the applicability of a biphasic computational formulation to describe the mechanics of cell-seeded protein hydrogels, a commonly used *in vitro* experimental model. The computational model was validated using experimentally determined and estimated material parameters in a confined compression test configuration. The analysis emphasized the importance of incorporating the Brinkman term to the biphasic formulation in order to accurately predict material behavior. The validated model was subsequently used to estimate the fluid pressure, relative fluid velocity, and von Mises stress distributions in gels exposed to different combinations of cyclic strain, cross flow, and combined strain and flow. These results have applicability to multiple studies that have applied cyclic deformation to cell-seeded hydrogels to create *in vitro* models of cartilage,[20] bone,[33] vasculature,[9] as well as other tissue types.

Confined compression was chosen to validate the model because the relevant geometry and boundary conditions are well defined and easily implemented computationally. Measuring the creep rate produced consistent experimental results. The control system for the uniaxial testing system maintained a constant load ±0.5 grams-force over the test interval, which provided uniformity when normalizing the creep rate to applied stress since the stress was averaged over the testing interval. Also, the geometry of the 2D model was created so that the aspect ratio matched the actual dimensions of the experimental collagen hydrogels. Under these conditions, inclusion of the Brinkman term in the biphasic model resulted in a close match to experimental results, whereas removal of the term caused the computational model to overestimate the creep rate by 35%. This disparity highlights the importance of viscous effects, since the resistance to deformation during creep is primarily from the viscous component of the material. Therefore, describing the viscosity of the fluid fraction of the biphasic model via the Brinkman term can more accurately model the viscous mechanics of the gel. Applying the model to a recently designed flow/strain apparatus further demonstrated the importance of the Brinkman term; the fluid pressure distributions for a 5% tensile strain cycle were compared with and without the addition of the viscous term. Adding the Brinkman term caused an asymmetry in the pressure distribution, with a peak in pressure occurring at the end of the gel being strained.

This study applies the biphasic formulation to a hydrogel consisting of a specific collagen density, seeded with a specific cell density. To make these results applicable to researchers using hydrogels with different native proteins (fibrin, Matrigel, etc.) or synthetic scaffolds (PLGA, PEG, etc.), different values of porosity and permeability were input into the model. It is possible that for materials with different porosity or permeability, the Brinkman term may not be as clearly relevant. In Fig. 5a, increasing the permeability by a factor of two attenuated the rise in pressure near the cycling end of the gel that distinguished the formulation with the Brinkman term in Fig. 4a. This result showed that there may exist a range of values for which the Brinkman term is unnecessary. Figure 4c addresses this issue by taking the ratio between the average pressure predicted by formulations with and without the Brinkman term. The effect of the Brinkman term on the solution increases as permeability decreases. This result is intuitive because at lower permeabilities, the solid

phase has greater relative surface area. This would increase the importance of accounting for viscous interactions between fluid and solid phases using the Brinkman term, as is reflected in the simulation results. Predicting the pressures, relative velocities, and solid stresses within mechanically stimulated hydrogels is important when analyzing the response of embedded cells. This holds true not only for the particular experimental configuration used in this study, but also more broadly for any system that applies solid or fluid stress to three-dimensional cell-seeded hydrogels. Cells are exposed to solid stress from the deformation of the matrix as well as shear stress from the flow of fluid within the gel. Models such as the one we have developed can therefore provide insight into the specific mechanical factors that affect cell function. In this study, we applied cyclic strain, cross flow, or a combination of both. The results indicated that although cyclic strain can induce fluid flow, imposing a cross flow causes negligible strain in a biphasic medium. In fact, the fluid velocity induced by 1 Hz cyclic strain was about 10 times higher than for a static gel exposed to cross flow for the same pressure difference across the gel. Similarly, the maximum von Mises stress for the cyclically strained gels (900 Pa) was about an order of magnitude higher than that of the cross-flow gels (90 Pa).

The results of the simulation indicate that for all three loading scenarios, cells embedded in hydrogels were exposed to some level of both interstitial fluid flow and structural strain. Combining cross flow and cyclic strain did not substantially affect the von Mises stress within the gels, but did affect the relative velocity in the *y* direction. Without cross flow, the relative fluid flow at the centerline of the gel in the *x* direction was zero, indicating no net fluid flow across the gel. Applying a common analogy between fluid flow and electric current, cyclic strain can be considered to induce an AC current while cross flow causes a DC offset to that current. Therefore, even though the effects of strain and cross flow are very much intertwined, the three loading scenarios of cyclic strain, cross flow, and a combination of both create three different stress states within the gels. Consequently, the response of cells imbedded in the gels should differ depending on which loading scenario is used.

This study highlights aspects of cell-seeded 3D collagen hydrogels that are of importance when using them used as *in vitro* models. The impact of the Brinkman term in our model shows that viscous effects in pure protein matrices can cause a fundamental difference in mechanical response, when compared to more dense native tissues. In addition, application of strain to such hydrogels induces interstitial fluid flow that acts in concert with the applied solid deformation, and these flows can be of a magnitude that affects cell behavior. Together these results suggest that applying mechanical strain to 3D protein hydrogels can induce mechanotransduction in embedded cells through strain, fluid shear, or a combination of both.

Acknowledgments

This study was supported in part by the Microfluidics in Biomedical Sciences Training Program at the University of Michigan, sponsored by the National Institute of Biomedical Imaging and Bioengineering.

References

1. Allen TD, Schor ST. The contraction of collagen matrices by dermal fibroblasts. J Ultrastruct Res. 1983; 83:205–219. [PubMed: 6864862]
2. Ateshian GA, Wang H, Lai WM. The role of interstitial fluid pressurization and surface porosities on the boundary friction of articular cartilage. J Tribol ASME. 1998; 120:241–251.
3. Bell E, Evarsson B, Merrill C. Production of a tissue-like structure by contraction of collagen lattices by human fibroblasts of different proliferative potential in vitro. Proc Natl Acad Sci. 1979; 76:1274–1278. [PubMed: 286310]

4. Bowen, R. Theory of mixtures. In: Eringen, AE., editor. Continuum Physics. Vol. 3. New York, NY: Academic Press; 1976. p. 1-127.
5. Breuls RGM, Sengers BG, Oomens CWJ, Bouten CVC, Baaijens FPT. Predicting local cell deformations in engineered tissue constructs: a multilevel finite element approach. J Biomech Eng. 2002; 124(2):198–208. [PubMed: 12002129]
6. Chan B, Donzelli PS, Spilker RL. A mixed-penalty biphasic finite element formulation incorporating viscous fluids and material interfaces. Ann Biomed Eng. 2000; 28:589–597. [PubMed: 10983705]
7. Chen X, Sarntinoranont M. Biphasic finite element model of solute transport for direct infusion into nervous tissue. Ann Biomed Eng. 2007; 35(12):2145–2158. [PubMed: 17846894]
8. Chevallay B, Herbage D. Collagen-based biomaterials as 3D scaffold for cell cultures: applications for tissue engineering and gene therapy. Med Biol Eng Comput. 2000; 38:211–218. [PubMed: 10829416]
9. Cummings CL, Gawlitta D, Nerem RM, Stegemann JP. Properties of engineered vascular constructs made from collagen, fibrin, and collagen–fibrin mixtures. Biomaterials. 2004; 25(17):3699–3706. [PubMed: 15020145]
10. Freed LE. Advanced tools for tissue engineering: scaffolds, bioreactors, and signaling. Tissue Eng. 2006; 12(12):3285–3305. [PubMed: 17518670]
11. Galie PA, Stegemann JP. Simultaneous application of interstitial flow and cyclic mechanical strain to a 3D cell-seeded hydrogel. Tissue Eng C. 2011; 17(5):527–536.
12. Galie PA, Westfall MV, Stegemann JP. Reduced serum content and increased matrix stiffness promote the cardiac myofibroblast transition in 3D collagen matrices. Cardiovasc Pathol. 2011 Epub ahead of print.
13. Ghosh K, et al. Cell adaptation to a physiologically relevant ECM mimic with different viscoelastic properties. Biomaterials. 2007; 28(4):671–679. [PubMed: 17049594]
14. Grinnell F. Fibroblast biology in three-dimensional collagen matrices. Trends Cell Biol. 2003; 13(5):264–269. [PubMed: 12742170]
15. Gudi SRP, Lee AA, Clark CB, Frangos JA. Equibiaxial strain and strain rate stimulate early activation of G proteins in cardiac fibroblasts. Am J Physiol Cell Physiol. 1998; 274(5):C1424–C1428.
16. Guilak F, Mow VC. The mechanical environment of the chondrocyte: a biphasic finite element model of cell– matrix interactions in articular cartilage. J Biomech. 2000; 33(12):1663–1673. [PubMed: 11006391]
17. Holmes MH. Finite deformation theory of soft tissue: analysis of a mixture model in uniaxial compression. J Biomech Eng. 1986; 108:372–381. [PubMed: 3795885]
18. Hou JS, Holmes MH, Lai WM, Mow VC. Boundary conditions at the cartilage-synovial fluid interface for joint lubrication and theoretical verifications. J Biomech Eng. 1989; 111:78–87. [PubMed: 2747237]
19. Kenyon DE. The theory of an incompressible solid–fluid mixture. Arch Ration Mech Anal. 1976; 62:131–147.
20. Kisiday J, Jin M, Kurz B, et al. Self-assembling peptide hydrogel fosters chondrocyte extracellular matrix production and cell division: implications for cartilage tissue repair. PNAS. 2002; 99(15): 9996–10001. [PubMed: 12119393]
21. Mak AK, Lai WM, Mow VC. Biphasic indentation of articular cartilage—I. Theoretical analysis. J Biomech. 1987; 20(7):703–714. [PubMed: 3654668]
22. McGuire S, Zaharoff D, Yuan F. Nonlinear dependence of hydraulic conductivity on tissue deformation during intratumoral infusion. Ann Biomed Eng. 2006; 34(7):1173–1181. [PubMed: 16791492]
23. Mow VC, Kuei SC, Lai WM, Armstrong CG. Biphasic creep and stress relaxation of articular cartilage in compression: theory and experiments. J Biomech Eng. 1980; 102:73–84. [PubMed: 7382457]
24. O'Brien FJ, Harley BA, Waller MA, Yannas IV, Gibson LJ, Prendergast PJ. The effect of pore size on permeability and cell attachment in collagen scaffolds for tissue engineering. Technol Health Care. 2007; 15:3–17. [PubMed: 17264409]

25. Ramanujan S, Pluen A, McKee TD, Brown EB, Boucher Y, Jain RK. Diffusion and convection in collagen gels: implications for transport in the tumor interstitium. Biophys J. 2002; 83:1650–1660. [PubMed: 12202388]

26. Slomka N, Or-Tzadikario S, Sassun D, Gefen A. Membrane-stretch-induced cell death in deep tissue injury: computer model studies. Cell Mol Bioeng. 2009; 2(1):118–132.

27. Spilker, RL.; Suh, JK.; Mow, VC. A finite element formulation of the nonlinear biphasic model for articular cartilage and hydrated soft tissues including strain-dependent permeability. In: Spilker, RL.; Simon, BR., editors. Computational Methods in Bioengineering. New York: ASME; 1982. p. 81-92.

28. Stegemann JP, Hong H, Nerem RM. Mechanical, biochemical, and extracellular matrix effects on vascular smooth muscle cell phenotype. J Appl Physiol. 2005; 98:2321–2327. [PubMed: 15894540]

29. Stegemann JP, Nerem RM. Phenotype modulation in vascular tissue engineering using biochemical and mechanical stimulation. Ann Biomed Eng. 2003; 31(4):391–402. [PubMed: 12723680]

30. Stops AJF, McMahon LA. A finite element prediction of strain on cells in a highly porous collagen-glycosaminoglycan scaffold. J Biomech Eng. 2008; 130(6):100–111.

31. Stylianopoulos T. Volume-averaging theory for the study of the mechanics of collagen networks. Comput Methods Appl Mech Eng. 2007; 196(31–32):2981–2990.

32. Wang DM, Tarbell JM. Modeling interstitial flow in an artery wall allows estimation of wall shear stress on smooth muscle Cells. J Biomech Eng. 1995; 117(3):358–364. [PubMed: 8618390]

33. Weinand C, Pomerantseva I, Neville CM, Gupta R, Weinberg E, Madisch I, Shapiro F, Abukawa H, Troulis MJ, Vacanti JP. Hydrogel-β-TCP scaffolds and stem cells for tissue engineering bone. Bone. 2006; 38(4):555–563. [PubMed: 16376162]

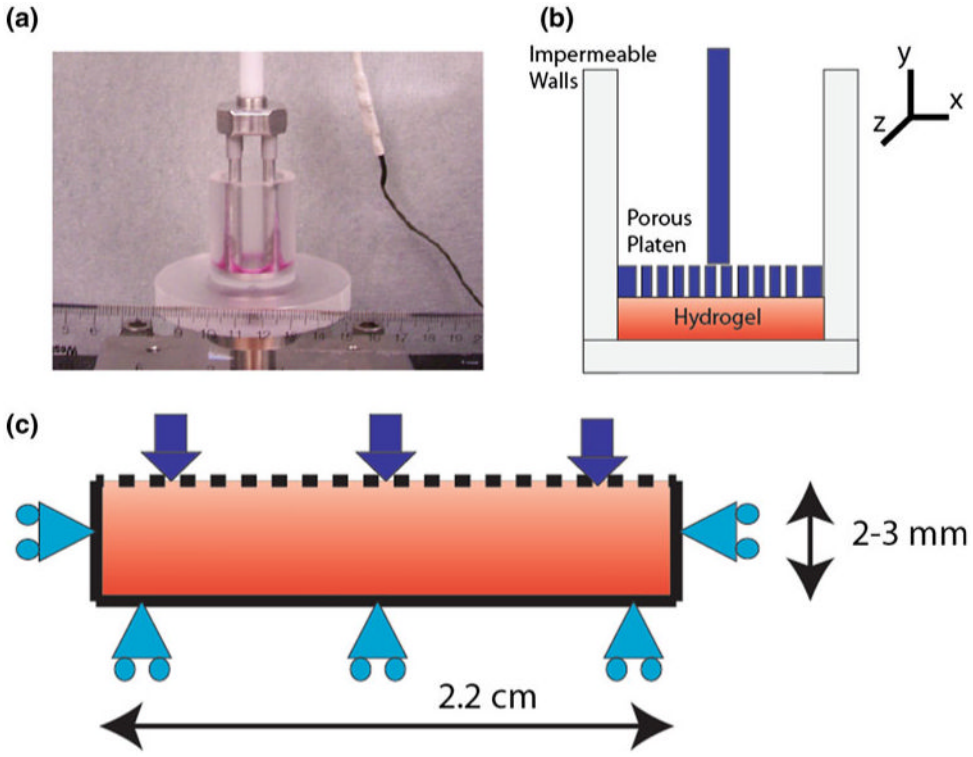

Figure 1.
Creep test validation. (a) Image of the confined compression system used for the creep testing. (b) Schematic of the platen and chamber. (c) The constant compressive force applied by the compression platen is represented by a row of arrows.

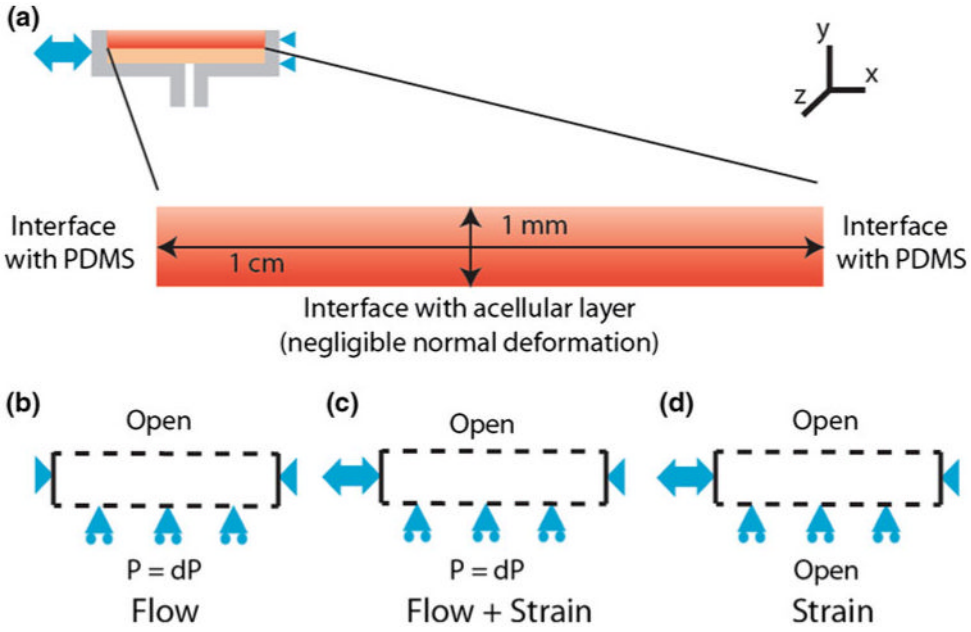

Figure 2.

(a) Schematic of the cell-seeded hydrogel within the PDMS flow/strain wells and its dimensions. The gel was bounded on both sides by PDMS, open to atmosphere at the top boundary, and attached to the acellular region on the bottom boundary. (b) Boundary conditions for application of cross flow: a dotted line represents an open boundary, a triangle denotes a boundary that is fixed in both the *x* and *y* directions, and a roller support restricts deformation only normal to the boundary. (c) Boundary conditions for cross flow and cyclic strain combined. The only difference between (b) and (c) is the addition of the cyclic strain condition on the left boundary. (d) Boundary conditions for cyclic strain only: both the top and bottom boundaries are open to fluid flow.

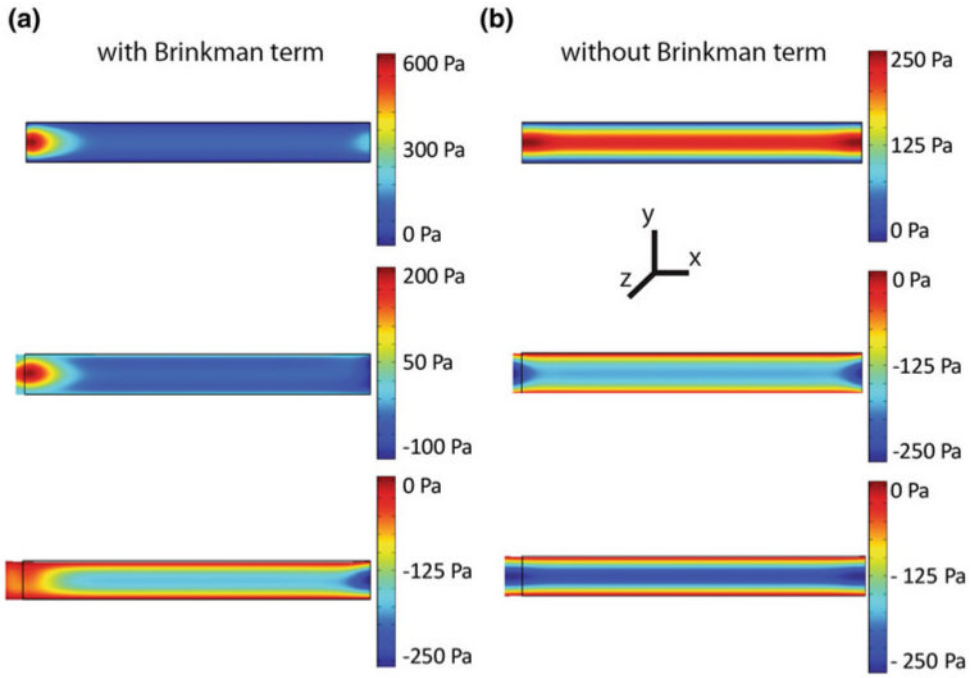

Figure 3.
Pressure contours with and without the incorporation of the Brinkman term. These contours are shown for three points in the strain cycle (top row: 0% strain, middle row: 2.5% strain, bottom row: 5% strain).

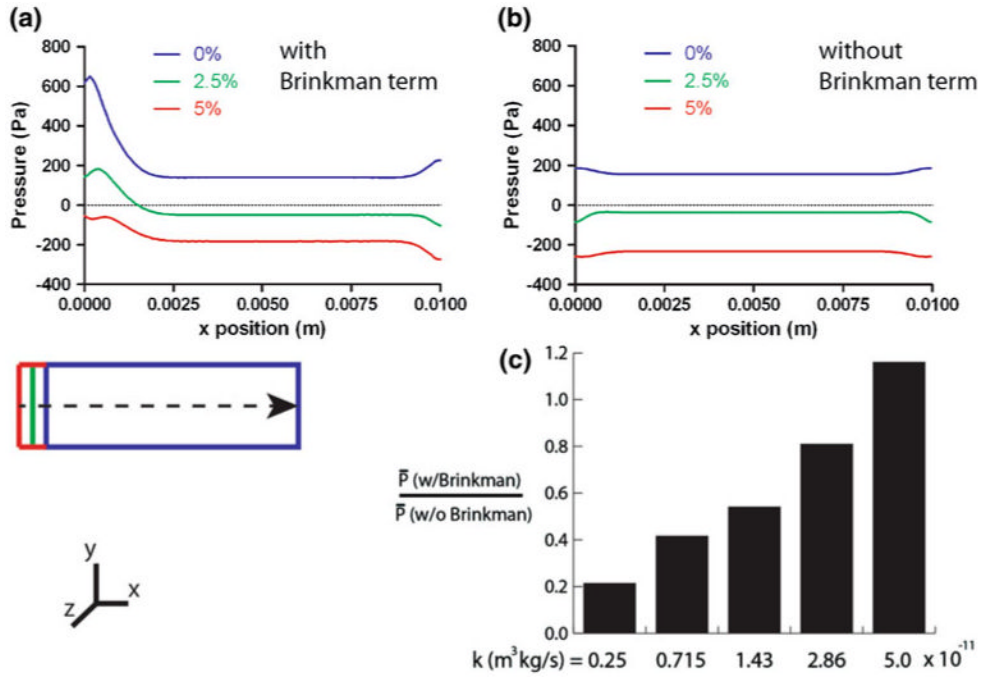

Figure 4.

Pressure distribution along the *x* axis at the midpoint of the gel for formulations with (a) and without (b) the viscous Brinkman term. The diagram in the bottom left-hand corner shows the direction of the arc-length along the gel, and the three points in the cycle are shown and are color-coded. (c) The ratio of predicted fluid pressure averaged over the length of the gel along the *y* axis centerline ($\bar{P}$) between formulations with and without the Brinkman term.

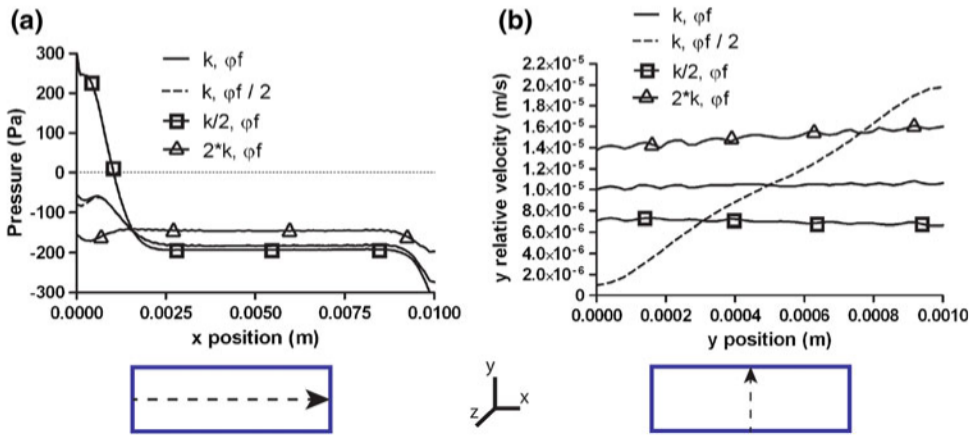

Figure 5.

(a) Pressure distribution along the *x* axis at the midpoint of the gel at 5% tensile train for four different sets of porosity and permeability values (solid line = original *k* and φ, dashed line = *k* and φ/2, square line = *k*/2 and φ, triangle line = 2*k* and φ). (b) *y* relative velocities along the *y* axis at the midpoint of the gel for the same four sets of parameter values.

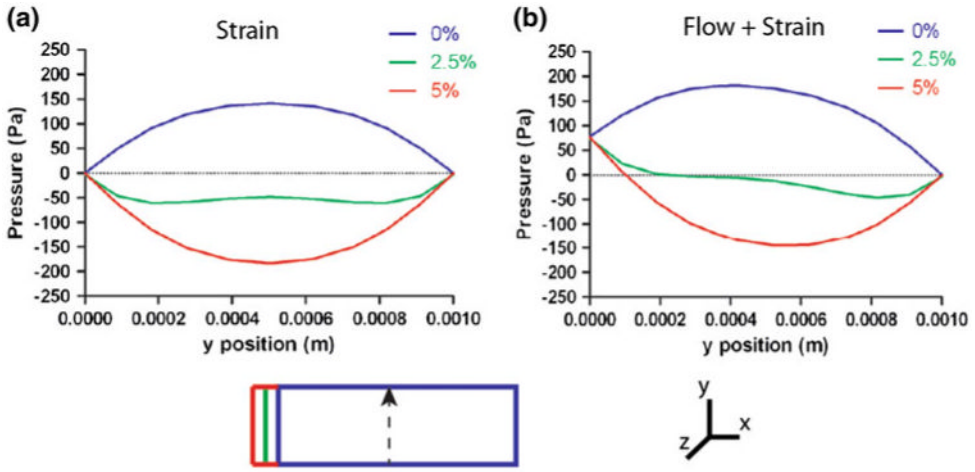

Figure 6.

Pressure distribution along the *y* axis at the midpoint of the gel for cyclically strained gels with (a) and without (b) the addition of cross flow. The imposed pressure gradient of 77.6 Pa is evident at zero arc-length in (b). Again, a diagram illustrates the direction of the arc-length and the three points of the cycle analyzed.

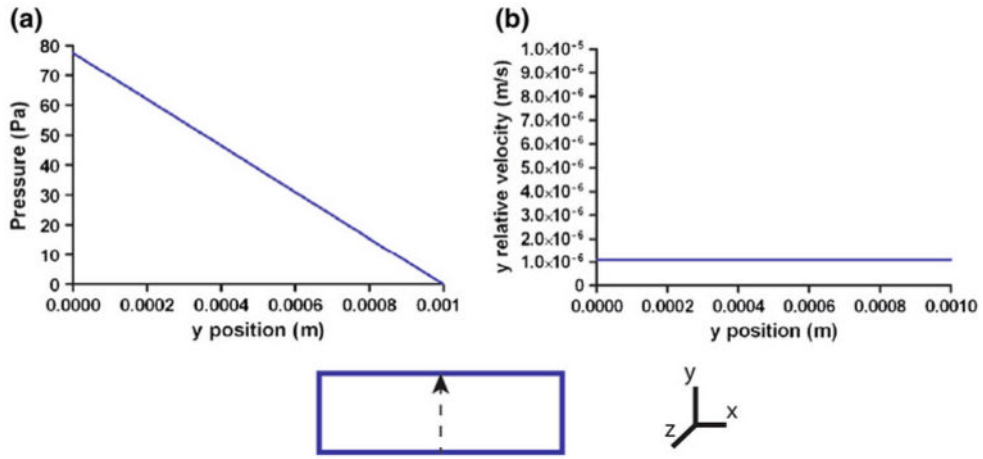

Figure 7.

Pressure drop (a) and *y* component of relative velocity (b) for the static, cross flow-only case. These distributions are taken along the *y* axis at the midpoint.

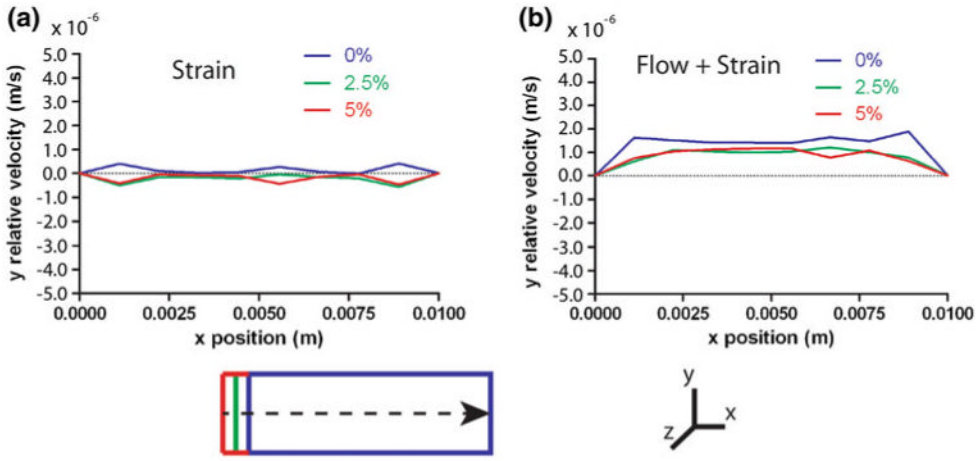

Figure 8.

Y component of relative fluid velocity along the *x* axis at the gel midpoint for cyclically strained gels with (a) and without (b) the addition of cross flow. Note that at the left and right ends of the gel (arc-length = 0, 0.01 m) the relative fluid velocity is constrained to zero.

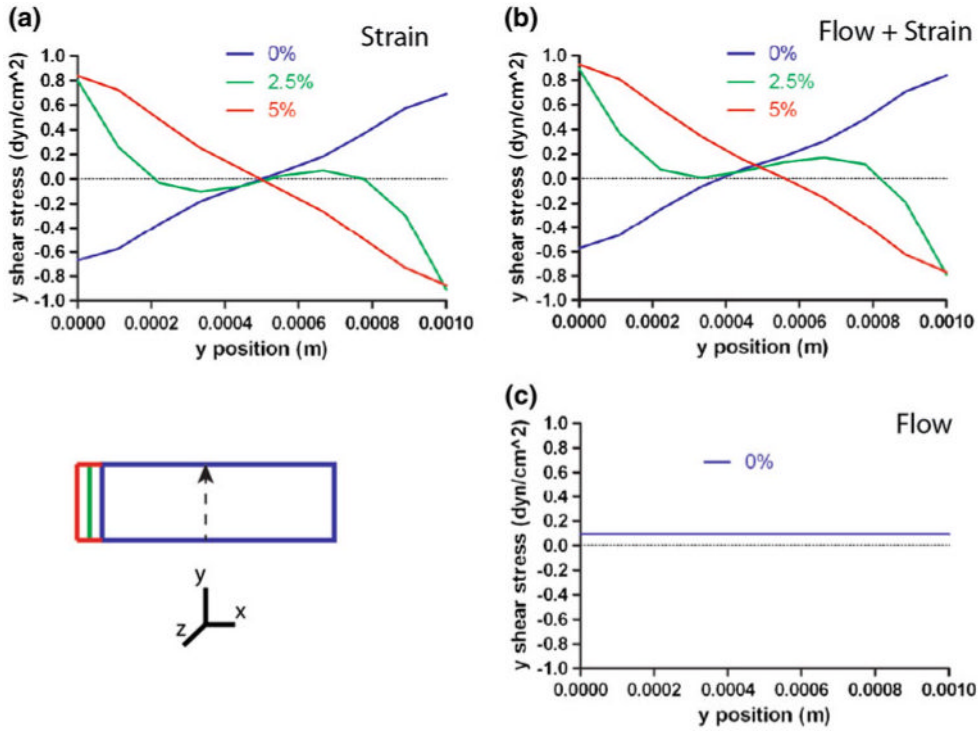

Figure 9.

Y component of shear stress along the *y* axis at the gel midpoint for cyclically strained gels with (a) and without (b) cross flow and static cross flow (c). The colors again correspond to the 0, 2.5, and 5% points in the loading cycle.

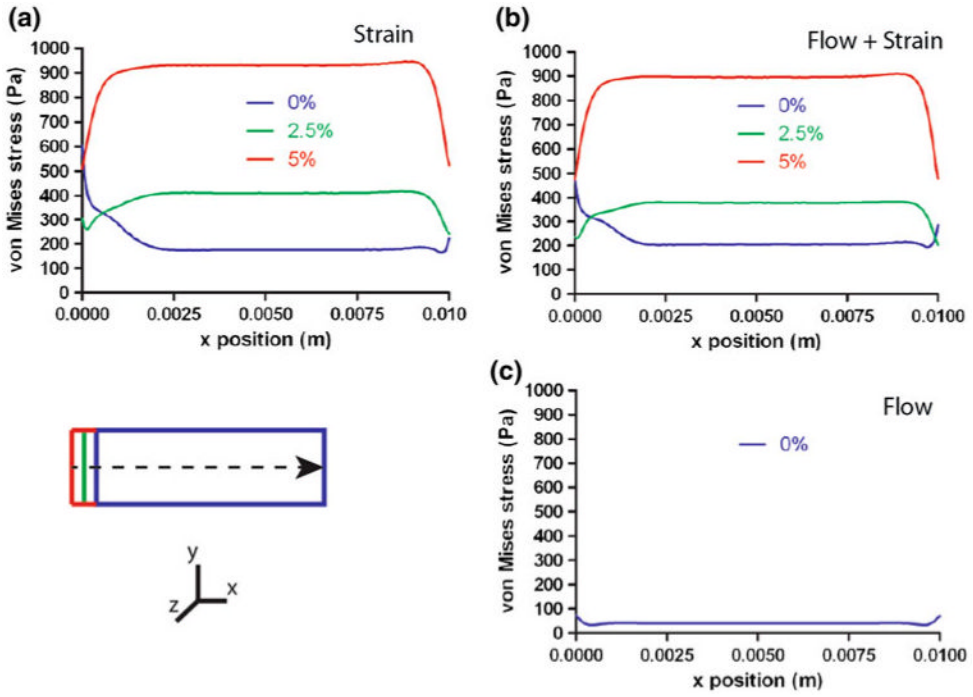

Figure 10.
von Mises stress distributions along the *x* axis at the gel midpoint for cyclically strained gels with (a) and without (b) cross flow and static cross flow (c).